Mechanisms of Extensive Spatiotemporal Chaos in Rayleigh-Bénard Convection

David A. Egolf[*,†], **Ilarion V. Melnikov**[*,‡], **Werner Pesch**[§], **and Robert E. Ecke**[*,†]

[*] *Center for Nonlinear Studies, Theoretical Division*
[†] *Condensed Matter & Thermal Physics, Los Alamos National Laboratory, Los Alamos, NM 87545, USA*
[§] *Theoretical Physics II, University of Bayreuth, Germany*

[‡] *Present Address: Department of Physics, Duke University*

Spatially-extended dynamical systems exhibit intriguing behavior that is complex in both space and time ("spatiotemporal chaos")[2,3]. Whereas insight into the crucial dynamical degrees of freedom in low-dimensional chaos has been routinely obtained through the analysis of dynamical quantities such as fractal dimensions and Lyapunov exponents[1], high-dimensional spatiotemporal chaos has proven quite difficult to understand despite abundant data describing its statistical properties[2,4,?]. Initial attempts to extend the dynamical approach to higher-dimensional systems demonstrated numerically that the spatiotemporal chaos in several simple models is extensive[8–10] in that the number of dynamical degrees of freedom scales with the system volume. Here we enumerate for the first time the dynamical degrees of freedom (of order 100) underlying spatiotemporal chaos exhibited by equations that accurately describe a phenomenon found in nature, Rayleigh-Bénard convection, in the Spiral Defect Chaos state[?,13] exhaustively studied in experiment. By studying the detailed space-time evolution of the dynamical degrees of freedom, we determine not only that the dynamics is extensively chaotic, but that the mechanism for the generation of chaotic disorder is spatially- and temporally-localized to defect creation/annihilation events.

The strong irregularity in both space and time observed in Rayleigh-Bénard convection is found in other complex dynamical systems such as heart tissue, nonlinear chemical and fluid patterns, planetary atmospheres and oceans, fluid turbulence, and environmental ecosystems. In some instances, the effective degrees of freedom in the problem (roughly, the average number of *independent* variables needed to describe the system) are thought to be extensive[8–10]. In others, new behaviors are found at all scales. In both cases, identifying the dynamical degrees of freedom and the instability mechanisms leading to disorder is of great importance. For example, better prediction of the nucleation and paths of tornadoes or hurricanes, the evolution of the global climate, or the transition to cardiac arrhythmia might be expected. Whereas scientists can often develop intuition by studying detailed experiments or large computer simulations, a general *quantitative* technique for identifying instability mechanisms leading to loss of predictability in physically-realizable, complex, spatially-extended systems has not been achieved. For developing and testing such methods, pattern formation in nonlinear, nonequilibrium systems is ideal because there are many high-precision laboratory experiments on pattern dynamics[2,?] and because numerical simulation of the evolution equations for such systems is within the grasp of present-day supercomputers. With such advances, the identification of dynamic mechanisms for complex spatially-extended systems can move beyond intuition towards a firm quantitative foundation.

Some of the most detailed experiments on complex dynamics in pattern-forming systems have studied Rayleigh-Bénard convection (RBC). An RBC experiment consists of a fluid layer of depth d confined between two horizontal conducting plates held at temperatures $T_{\rm top}$ and $T_{\rm bottom}$. For temperature differences $\Delta T = T_{\rm bottom} - T_{\rm top}$ less than a critical temperature difference ΔT_c, the fluid is stationary. When $\Delta T > \Delta T_c$, the stationary state is unstable and the fluid begins to flow[?] with the "distance" from the onset of flow expressed as $\epsilon = \Delta T/\Delta T_c - 1$. For systems with small aspect ratios (lateral dimension L relative to d), the flow is typically organized into parallel convective "rolls" of diameter approximately equal to d, with each roll consisting of hot fluid moving upward on one side and cold fluid moving downward on the other. The convective flow carries heat and enhances heat transport, making convection an important process in the atmosphere and oceans and in many technological applications. For large aspect ratios (L/d of order 100), Morris, *et al*[13] discovered the persistent state of Spiral Defect Chaos (SDC) consisting of locally parallel rolls arranged in temporally-chaotic, spatially-complex patterns. This initial work led to many additional experiments yielding a large quantity of high-precision data[?]. In these experiments, the complex two-dimensional convective patterns are visualized using the optical shadowgraph technique[11]. Virtually indistinguishable patterns (e.g., Fig. 1) are observed in simulations of the Boussinesq equations, the standard hydrodynamic equations describing convection[12]. The patterns have been characterized by global Fourier transform methods[13,14,5,6], with local roll properties such as curvature and wavenumber variations[5,6,15], and by the statistics of spiral-defect populations[15,7]. Researchers have also studied the mechanism of spiral creation and stability both experimentally and theoretically[16–18]. Despite this formidable effort, the direct dynamical degrees of freedom are unknown.

A common method for quantifying the dynamics of nonlinear systems is to study the evolution of states that are nearly identical to a reference state. The divergences of these states from the reference state are characterized by a set of exponents called the Lyapunov spectrum $\lambda_1 > \lambda_2 > \ldots$[1]. Each Lyapunov exponent λ_i corresponds to a Lyapunov vector, which is simply a particular perturbation (out of all of the possible choices of perturbations) away from the reference state, and each Lyapunov vector is orthogonal to all of the others. Each Lyapunov exponent

FIG. 1. Instantaneous temperature field of Rayleigh-Bénard convection for $\epsilon = 0.8$ showing the state of spiral defect chaos.

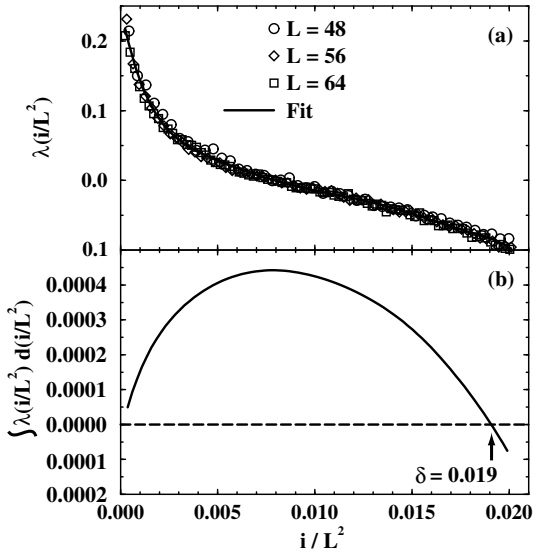

FIG. 2. a) Spectrum of Lyapunov exponents λ_i vs system-size-normalized index i/L^2 for $\epsilon = 0.8$ and L: 48 ($\circ$), 56 ($\diamond$), 64 ($\square$). The solid line is a 7th-degree polynomial fit to the data. b) Integral of the Lyapunov spectral density $\lambda(i/L^2)$ vs i/L^2 computed from the curve fit in a). The dimension density $\delta \approx 0.019$ is determined by the zero intercept of the data.

quantifies the average exponential rate of growth of the perturbation represented by the corresponding Lyapunov vector. For RBC, the perturbations represented by the Lyapunov vectors are small differences in the temperature and/or velocity fields with respect to a reference state exhibiting SDC. The evolution of the reference state is computed using the Boussinesq equations, and the evolutions of the Lyapunov vectors are computed according to the linearization of the Boussinesq equations about the time-dependent reference state. (The linearized equations ensure that the exponents describe the divergence of states that differ only infinitesimally from the reference.) The "direction" of each Lyapunov vector characterizes the spatial distribution of perturbations in the temperature and velocity fields (with each component of the vector representing the perturbation at a particular point in space for the temperature or velocity fields).

The (fractal) Lyapunov dimension D is a measure of the complexity of the dynamics (or, in other words, how chaotic the system is) and can be calculated by the Kaplan-Yorke formula which expresses D in terms of the Lyapunov exponents λ_i. From arguments first given by Ruelle[8], we expect that in large systems distant regions will be dynamically independent, so D will grow in proportion to the volume L^{d_s}, where d_s is the spatial dimensionality ($d_s = 2$ for SDC) and L is the lateral length scale; *i.e.*, the dimension is extensive with intensive dimension density $\delta = D/L^{d_s}$. This chaotic extensivity can be phrased in stronger terms by studying the Lyapunov spectral density $\lambda(i/L^{d_s})$ as $L \to \infty$ (where i is the same index as in λ_i). For extensively chaotic systems $\lambda(i/L^{d_s})$ becomes invariant. Even for relatively low-dimensional dynamical systems it is extremely difficult to measure enough Lyapunov exponents from experimental data to compute D. Thus, researchers studying spatiotemporal chaos have turned to relatively simple spatially-extended model systems such as the Kuramoto-Sivashinsky equation[9] and the complex Ginzburg-Landau (CGL) equation[10] for which simple but computationally intensive methods have allowed the computation of the Lyapunov spectra for several different system sizes L. For these systems, the chaotic dynamics was convincingly demonstrated to be extensive.

To test whether an actual experimental system exhibits extensive chaos, we studied the Boussinesq equations computationally. Even though several simple models exhibit extensive chaos, it is not obvious *a priori* that the chaos in RBC is extensive. RBC differs from the simple models in significant ways. In RBC, pressure modes that act instantaneously and decay slowly in space could couple distant spatial regions. Also, simple non-chaotic RBC states exist for the same experimental parameters at which spatiotemporal chaos is found[7].

We integrated the Boussinesq equations using a pseudospectral method with time-splitting of the operators. To minimize boundary effects and emphasize bulk properties, periodic boundary conditions were employed. Our code is consistent with exact linear and weakly-nonlinear results. We verified numerical convergence with respect to spatial and temporal resolutions and integration times. The Lyapunov spectrum was obtained by simultaneously evolving up to $N = 128$ orthogonal fields (the Lyapunov vectors) according to the linearization of the Boussinesq equations about a particular solution exhibiting SDC. The N Lyapunov vectors are the N (orthogonal) perturbations with the largest average growth rates λ_i. Further details are provided elsewhere (In preparation).

Fig. 2a shows the Lyapunov spectral density $\lambda(i/L^2)$ for the Spiral Defect Chaos state of RBC at $\epsilon = 0.8$. The Lyapunov spectral densities for system sizes $L = 48, 56$, and 64 collapse onto a single curve, demonstrating unambiguously

that SDC is extensive. These data represent the first direct demonstration of the principle of extensivity of the *dynamics* of an experimentally-relevant spatiotemporal chaotic system. The value of the dimension density δ is calculated using the Kaplan-Yorke formula as the value of i/L^2 such that the area under the curve shown in Fig. 2a from 0 to $\delta = i/L^2$ is zero. This procedure is shown schematically in Fig. 2b and yields $\delta = 0.019$ (in units of d^{-2}) corresponding to a fractal dimension $D \approx 80$ for L=64. We note that the number of dynamical degrees of freedom ($\sim 10^2$) is smaller by several orders of magnitude than the number of spatial modes obtained by orthogonal decomposition ($\sim 10^4$ using either Karhunen-Loeve[19] or Fourier methods). It is the same order of magnitude, however, as estimates[14] from experiments ($D \approx 200$) based on measured correlation lengths and adjusted for our system size.

Because the Lyapunov spectrum is an infinite-time average, the intriguing dynamical behavior of the underlying Lyapunov vectors is often overlooked. The spatial distributions of the perturbations, as well as their growth rates, vary substantially in time. The growth rates are quantified by the *time-dependent* finite-time Lyapunov spectrum of exponents $\lambda_i^{(\Delta\tau)}(t)$ describing the exponential divergence of similar states over the interval $(t, t+\Delta\tau)$. The time-dependent Lyapunov vector directions (spatial distributions of perturbations) and finite-time Lyapunov exponents reflect the dynamical features within the evolution of the system itself[20,21]. Here we study the dynamical degrees of freedom in greater detail by comparing the space-time structures of the Lyapunov vectors to the evolution of the system in order to reveal the mechanism of the spatiotemporal chaos in RBC.

For our system, the positive Lyapunov exponents correspond to highly-localized vectors, whereas the zero and negative exponents correspond to vectors that are more homogeneously distributed in space. The localization of the Lyapunov vectors with positive exponents is correlated with regions of the pattern that are linearly unstable due to the rolls being too narrow or too wide[15,22]. The finite-time Lyapunov exponents have considerable fluctuations with the largest positive Lyapunov exponents having the greatest standard deviations. The highest maxima in the time sequences of finite-time exponents correspond to dramatic defect nucleation events. Fig. 3a shows the magnitudes of the temperature field components of the Lyapunov vector corresponding to the largest Lyapunov exponent, suitably scaled and color-coded to represent local magnitude (red being highest, blue smallest). Much of the pattern is quiescent but there is a strong event in the lower left. This localization is common for the vectors corresponding to positive Lyapunov exponents ("chaotic") and is further evidence for the Ruelle picture of extensive chaos — a doubling of the system size simply results in new Lyapunov vectors localized to the newly-added area of the system.

Fig. 3b-e show an expanded, time-ordered view of a particular event in Fig. 3a. The largest finite-time Lyapunov exponent quickly builds (Fig. 3b,c) to a maximum (Fig. 3d) at the moment of roll-breaking, followed by a rapid relaxation (Fig. 3e) to a negative value. The Lyapunov vector is

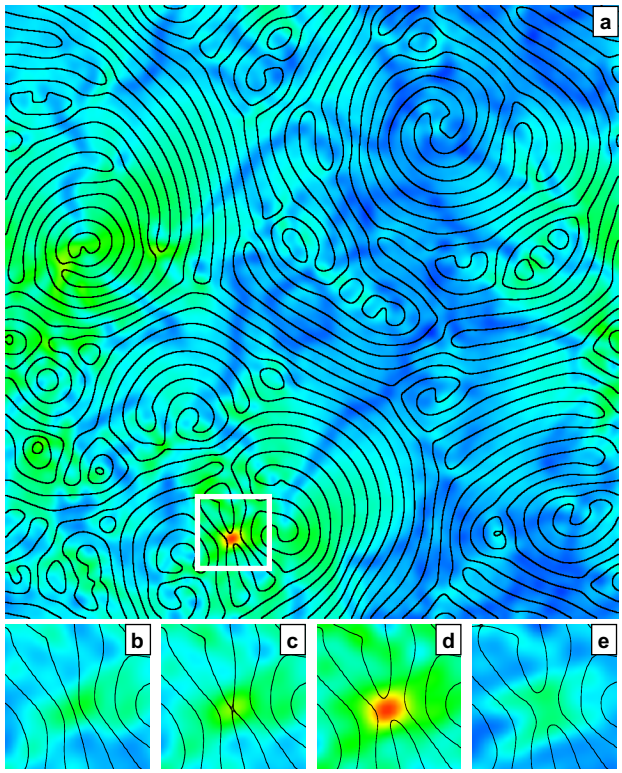

FIG. 3. First Lyapunov vector scaled by the first finite-time exponents, color-coded by magnitude, and superimposed on the underlying roll pattern. a) Whole 64×64 pattern, b) blown-up section $\Delta t = 0.3750\tau_v$ before a); c) blown-up section $\Delta t = 0.1875\tau_v$ before a); d) blown-up section of a); e) blown-up section $\Delta t = 0.1875\tau_v$ after a). The color scale (blue-cyan-green-yellow-red) is linear in the 1/4 power of the magnitude of the scaled vector. The size of the box is about one chaotic domain $\xi_\delta^2 = L^2/D$.

strongly localized to the small spatial region at which the breakage occurs, signifying that the evolution of the system is highly susceptible to small perturbations in this particular region, with minute details of the state determining the exact breaking point and defect motions and ultimately the future dynamics of the system. (In contrast, small differences between states in regions away from roll breaking/reconnection events will decay exponentially.) After the rolls break/reconnect, the dynamics of this Lyapunov vector is mostly relaxational as the defects diffuse away. This scenario of strong localization of the Lyapunov vector and positive spikes in the finite-time Lyapunov exponent correlated with roll breaking/reconnection events is intermittently repeated throughout the chaotic evolution of the system. (The strongly chaotic events include not only defect-generating skewed varicose events shown in Fig. 3, but also cross-roll events in regions of large local wavenumber[22].)

These data demonstrate that the mechanism generating the chaotic dynamics in the SDC state of RBC is roll breaking/reconnection rather than the more apparent motion of

the large spiral defects (in direct contrast to the active cores of chemical spirals). This mechanism for the generation of chaotic disorder makes intuitive sense because major roll reorientations occur via roll breaking/reconnection. Thus, the disorder in the patterns arises from the complicated regions between the spirals rather than in the spirals themselves (although the spirals may contribute to the generation of the complicated regions).

With sufficient computer power, the analysis technique described here is applicable to many complex problems for which the evolution equations are well-known or well-approximated. Although no methods for obtaining Lyapunov vectors from experimental data currently exist, this type of analysis might be possible in the not-so-distant future using an experimental technique to repeatedly recreate particular chaotic states or an analysis technique based on recurring substates.

Understanding the instability mechanisms of complex dynamical systems such as the global climate, ecological systems, fluid and chemical systems, financial markets, and large-aperture lasers would help immensely in controlling their spatiotemporal dynamics, in determining their long-time behavior, and in engineering systems to avoid or limit instabilities. Application of the techniques presented here to fibrillation patterns in the heart or to fully-developed three-dimensional turbulence are attainable using present-day computers.‘

[1] Eckmann, J.-P. & Ruelle, D. Ergodic-theory of chaos and strange attractors. *Rev. Mod. Phys.* **57**, 617-656 (1985).

[2] Cross, M.C. & Hohenberg, P.C. Pattern-formation outside of equilibrium. *Rev. Mod. Phys.* **65**, 851-1112 (1993).

[3] Cross, M.C. & Hohenberg, P.C. Spatiotemporal chaos. *Science* **263**, 1569-1570 (1994).

[4] For a review of some fluid systems, see, e.g., Gollub, J.P. Order and disorder in fluid motion. *Proc. Nat. Acad. Sci. (U.S.A.)* **92**, 6705-6711 (1995).

[5] Hu, Y., Ecke, R.E. & Ahlers, G. Transition to spiral-defect chaos in low Prandtl number convection. *Phys. Rev. Lett.* **74**, 391-394 (1995).

[6] Hu, Y., Ecke, R.E. & Ahlers, G. Convection for Prandtl numbers near 1: Dynamics of textured patterns. *Phys. Rev. E* **51**, 3263-3279 (1995).

[7] Ecke, R.E., Hu, Y., Mainieri, R. & Ahlers, G. Excitation of spirals and chiral-symmetry breaking in Rayleigh-Bénard convection. *Science* **269**, 1704-1707 (1995).

[8] Ruelle, D. Large volume limit of the distribution of characteristic exponents in turbulence. *Commun. Math. Phys.* **87**, 287-302 (1982).

[9] Manneville, P., Liapunov Exponents for the Kuramoto-Sivashinsky Model, 319-326 (*Lecture Notes in Physics* Vol. 230, Springer, Berlin, 1985).

[10] Egolf, D.A. & Greenside, H.S. Relation between fractal dimension and spatial correlation length for extensive chaos. *Nature* **369**, 129-131 (1994).

[11] de Bruyn *et al*, G. Apparatus for the study of Rayleigh-Bénard convection in gases under pressure. *Rev. Sci. Instrum.* **67**, 2043-2067 (1996).

[12] Decker, W., Pesch, W. & Weber, A. Spiral defect chaos in Rayleigh-Bénard convection. *Phys. Rev. Lett.* **73**, 648-651 (1994).

[13] Morris, S.W., Bodenschatz, E., Cannell, D. S. & Ahlers, G. Spiral defect chaos in large aspect ratio Rayleigh-Bénard convection. *Phys. Rev. Lett.* **71**, 2026-2029 (1993).

[14] Morris, S.W., Bodenschatz, E., Cannell, D. S. & Ahlers, G. The spatiotemporal structure of spiral-defect chaos. *Physica D* **97**, 164-179 (1996).

[15] Egolf, D.A., Melnikov, I.V. & Bodenschatz, E. Importance of local pattern properties in spiral defect chaos. *Phys. Rev. Lett.* **80**, 3228-3231 (1998).

[16] Assenheimer M. & Steinberg V. Transition between spiral and target states in Rayleigh-Bénard convection. *Nature* **367**, 345-347 (1994).

[17] Cross, M.C. & Tu, Y. Defect dynamics for spiral chaos in Rayleigh-Bénard convection. Phys. Rev. Lett. **75**, 834-837 (1995).

[18] Plapp B.B, Egolf, D.A., Bodenschatz, E. & Pesch, W. Dynamics and selection of giant spirals in Rayleigh-Bénard convection. *Phys. Rev. Lett.* **81**, 5334-5337 (1998).

[19] Zoldi, S.M., Liu, J., Bajaj, K.M.S., Greenside, H.S., & Ahlers, G. Extensive scaling and nonuniformity of the Karhunen-Loeve decomposition for the spiral-defect chaos state. *Phys. Rev. E* **58**, R6903-R6906 (1998).

[20] Chaté, H. Lyapunov analysis of spatiotemporal intermittency. *Europhys. Lett.* **21**, 419-425 (1993).

[21] Egolf, D.A. Dynamical dimension of defects in spatiotemporal chaos. *Phys. Rev. Lett.* **81**, 4120-4123 (1998).

[22] Busse, F.H. & Clever, R.M. Instabilities of convection rolls in a fluid of moderate Prandtl number. *J. Fluid Mech.* **91**, 319-335 (1979).

Acknowledgments. We acknowledge helpful discussions with E. Bodenschatz and R. Mainieri. This work was funded by the U.S. Department of Energy under contract W-7405-ENG-36, and significant computational resources were provided on the Nirvana machines of the Advanced Computing Laboratory at Los Alamos National Laboratory. The development of a related version of the Boussinesq equation solver benefited from the support of NSF Grant DMR-9705410.

Correspondence and requests for materials should be addressed to D.A.E (e-mail: egolf@lanl.gov).